nature chemical engineering

Article

https://doi.org/10.1038/s44286-024-00063-z

Molar-scale formate production via enzymatic hydration of industrial off-gases

Received: 28 August 2023

Accepted: 24 March 2024

Published online: 7 May 2024

Check for updates

Jinhee Lee[1,7], Suk Min Kim[1,7] ✉, Byoung Wook Jeon[1], Ho Won Hwang[1], Eleni G. Poloniataki[1], Jingu Kang[1], Sanghyung Lee[2], Ho Won Ra[3], Jonggeol Na[4], Jeong-Geol Na[5], Jinwon Lee[5] & Yong Hwan Kim[1,6] ✉

Decarbonizing the steel industry, a major CO_2 emitter, is crucial for achieving carbon neutrality. Escaping the grip of CO combustion methods, a key contributor to CO_2 discharge, is a seemingly simple yet formidable challenge on the path to industry-wide net-zero carbon emissions. Here we suggest enzymatic CO hydration (enCOH) inspired by the biological Wood–Ljungdahl pathway, enabling efficient CO_2 fixation. By employing the highly efficient, inhibitor-robust CO dehydrogenase (*Ch*CODH2) and formate dehydrogenase (*Me*FDH1), we achieved spontaneous enCOH to convert industrial off-gases into formate with 100% selectivity. This process operates seamlessly under mild conditions (room temperature, neutral pH), regardless of the CO/CO_2 ratio. Notably, the direct utilization of flue gas without pretreatment yielded various formate salts, including ammonium formate, at concentrations nearing two molar. Operating a 10-liter-scale immobilized enzyme reactor feeding live off-gas at a steel mill resulted in the production of high-purity formate powder after facile purification, thus demonstrating the potential for decarbonizing the steel industry.

The steel/iron industry (7% of global CO_2 emissions)[1] is one of the primary contributors to greenhouse-gas emissions in the manufacturing field, along with electricity generation and transportation[2,3]. With the increasing demand for steel and iron predicted to continue, substantial reductions in CO_2 emissions are imperative (annually 3 $GtCO_2$ emission by 2050)[2,4,5]. A major portion of these emissions originates from the combustion of CO, a by-product of iron production, releasing two tons of CO_2 per ton of manufactured steel[2,4,6]. Because of the toxicity of CO, its current method of disposal through combustion results in considerable CO_2 discharge, exacerbating emissions. This reliance on combustion also foregoes the potential to utilize CO as a feedstock for synthesizing alternative fuels and chemicals, thereby missing a critical opportunity to replace fossil resources with more sustainable options. Hence, the capture or transformation of CO into value-added compounds without resorting to combustion is emerging as a prospective solution towards industry-wide decarbonization and, by implication, a substantial reduction in CO_2 emissions.

The conversion of CO gas into commodity chemicals can be facilitated by metal-catalyzed chemical processes[7,8]. Among the two prevalent reactions, Fischer–Tropsch synthesis performed on syngas streams has emerged as a possible conduit for converting CO from the steel and iron industry[9,10], as opposed to the CO_2-generating water–gas-shift reaction. Nevertheless, these processes require harsh operational conditions and high energy inputs/capital costs, in addition to requiring high-purity CO gas. In contrast, bioconversion of CO is performed under milder conditions, thus demanding potentially lower energy input. Several pioneering advancements have demonstrated the efficacy of biocatalytic CO utilization, including LanzaTech's

[1]School of Energy and Chemical Engineering, Ulsan National Institute of Science and Technology (UNIST), Ulsan, Republic of Korea. [2]Environment and Energy Research Team, Research and Development Center, Dangjin, Republic of Korea. [3]Climate Change Research Division, Korea Institute of Energy Research (KIER), Daejeon, Republic of Korea. [4]Department of Chemical Engineering and Materials Science, Ewha Womans University, Seoul, Republic of Korea. [5]Department of Chemical and Biomolecular Engineering, Sogang University, Seoul, Republic of Korea. [6]Graduate School of Carbon Neutrality, Ulsan National Institute of Science and Technology (UNIST), Ulsan, Republic of Korea. [7]These authors contributed equally: Jinhee Lee, Suk Min Kim. ✉e-mail: smkimlife@unist.ac.kr; metalkim@unist.ac.kr

https://doi.org/10.1038/s44286-024-00063-z

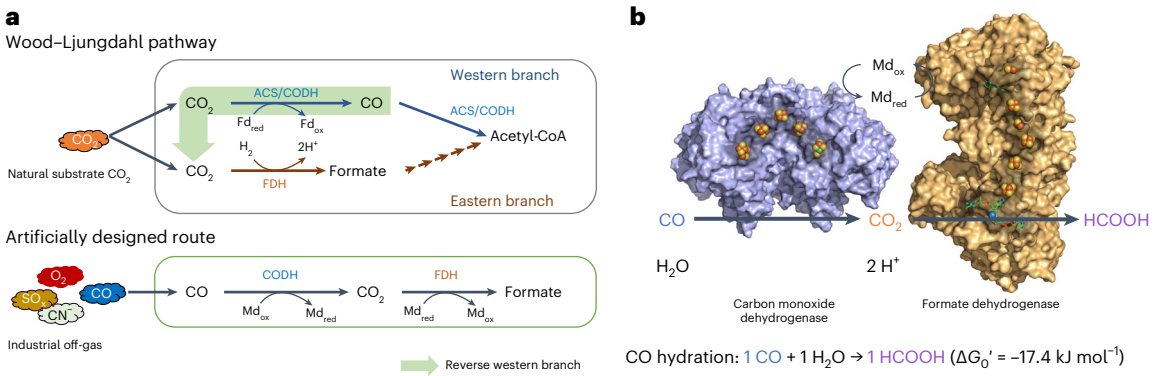

Fig. 1 | Illustration of enCOH. a, Conceptual overview of in vitro enCOH. This is inspired by the integration of the reverse western and eastern branches of the microbial WL pathway. **b**, Scheme of enCOH. CO is oxidized to CO_2 by CODH, and CO_2 is reduced to formate by FDH. The electron mediator (Md) transfers electrons between both enzymes. ACS, acetyl-CoA synthetase; Fd, ferredoxin; ox, oxidized; red, reduced.

ethanol fermentation and the Muller group's formate production via H_2-dependent CO_2 reductase (HDCR), both of which are derived from the acetogenic Wood–Ljungdahl (WL) pathway[11,12]. LanzaTech's process efficiently transforms low-cost waste gases into chemicals like ethanol, acetone and isopropanol using engineered acetogens, while the HDCR method uniquely converts CO_2 to formic acid using H_2 and electron transfer. The WL pathway, with its linear progression from CO_2 to formic acid (eastern branch) and CO (western branch)[13,14], presents a simpler implementation route compared to intricate circular CO_2 fixation cycles, such as the Calvin Benson Bassham cycle (involving multiple enzymes and reactions; Supplementary Fig. 1)[15]. Its application appears particularly promising for sulfur-containing off-gases, as the WL pathway's enzymes have evolved in sulfur-rich environments[16,17]. Despite these promising strides, obstacles still remain. For example, oxygen and toxic substances such as cyanide can impair stability, and the H_2-dependent carbon fixation yield for complete carbon utilization poses further challenges. Although HDCR represents a promising system for CO_2 conversion, it demands a continuous hydrogen supply to transform CO_2 effectively. Bioconversion of industrial off-gas necessitates addressing issues such as inhibition by gas impurities (CN^-, SO_x, NO_x and O_2), lower carbon yields and slower conversion rates at lower CO concentrations[15,18–25].

To address these challenges, we suggest an engineered in vitro enzymatic reaction inspired by the reverse western branch of the WL pathway to efficiently exploit industrial CO off-gas containing varied gas components and toxic impurities (Fig. 1a):

$$\text{Reverse western branch}: \ CO + H_2O \rightarrow CO_2 + 2e^- + 2H^+$$

(catalyzed by CO dehydrogenase)

$$\text{Eastern branch}: \ CO_2 + 2e^- + 2H^+ \rightarrow HCOOH$$

(catalyzed by formate dehydrogenase)

The designed reaction demonstrates favorable thermodynamics, presenting a promising route for the direct utilization of real industrial off-gas. Importantly, our enzyme-catalyzed CO hydration (enCOH) reaction, formulated as CO + H_2O → HCOOH (formic acid), occurs without any additional CO_2 emission (Fig. 1b). The standard Gibbs free energy of the enCOH reaction, $\Delta G_0' = -17.4$ kJ mol^{-1} at 25 °C and pH 7.0, further substantiates its thermodynamic feasibility (Supplementary Table 1). The toxic impurities typically found in flue gas (such as SO_x, NO_x, H_2S and CN^-) that usually deactivate metal catalysts and require complex and expensive pre-separation processes[26–29] surprisingly exert negligible inhibition effects on either the CO dehydrogenase (CODH) or formate dehydrogenase (FDH) involved in the enCOH reaction (Supplementary Fig. 2), making it facilely applicable to direct industrial off-gas. Therefore, the enCOH in vitro system has potential due to its ease of control, reduced complexity, simplicity in terms of engineering and optimization, and flexibility under various conditions.

In this Article we report an enCOH reaction that is operational at atmospheric temperature and pressure, facilitating molar-scale formate production from industrial steel manufacturing off-gas and waste-plastic gasification. This process exhibits enduring stability in both laboratory settings and a semi-pilot-scale installation within a steel mill's operational field.

Enzymatic hydration of CO to formate

The enCOH reaction initiates with CO as the starting substrate, leading to CO_2 production through CO oxidation catalyzed by CODH. The subsequent spontaneous reaction catalyzed by FDH results in the generation of formic acid, with a theoretical yield of 1 mole of formic acid per 1 mole of CO (Fig. 1b). To ensure efficient enCOH, it is preferable that a complete cycle reaction take place through the regeneration of the electron mediator in the preceding one-pot reaction. Natural electron carriers (such as ferredoxins) are too specific and are also oxygen-sensitive[30], so artificial options were examined for both CODHs and FDHs originated from various strains (Supplementary Table 2). Accordingly, the various viologens (methyl viologen (MV); benzyl viologen (BV); ethyl viologen (EV)) and a natural mediator (nicotinamide adenine dinucleotide (NAD)) were investigated based on their reaction energies, which were calculated based on the redox potential and standard Gibbs free energy at pH 7 (Supplementary Table 1 and Supplementary Fig. 3). These investigations suggested MV and EV to be more efficient mediators than BV or NAD, as they could supply enough energy to convert CO_2 to formate.

In our enCOH in vitro system, we selected candidate enzymes for CODH and FDH considering key parameters such as reactivity, substrate affinity, protein productivity and the pH optimum (Supplementary Table 3): *Carboxydothermus hydrogenoformans* (*Ch*)CODH2[31] was considered for its high CO-oxidizing activity, *Ch*CODH4[32] for its high CO affinity, *Thermococcus onnurineus* NA1 (*To*)CODH[33] for its broad pH range, *Methylobacterium extorquens* (*Me*)FDH1[23,34] for its high CO_2-reducing activity, *Rhodobacter capsulatus* (*Rc*)FDH[35,36] for its high CO_2 affinity and *Thiobacillus* sp. KNK65MA (*Ts*)FDH[37,38] for its high expression and efficiency. Acetogen-derived CODH was excluded due to its low CO_2-reducing activity in *Escherichia coli* (<0.04 U mg^{-1} for both NADH and EV_{red}; 0.14 U mg^{-1} from the Müller group[39]). Unlike CODH, which mostly has a negligible backward reaction, for FDH we considered the relative rates ($k_{cat,CO_2}/k_{cat,HCOO^-}$) of the forward ($CO_2$ reduction) and backward (formate oxidation) reactions (Supplementary

https://doi.org/10.1038/s44286-024-00063-z

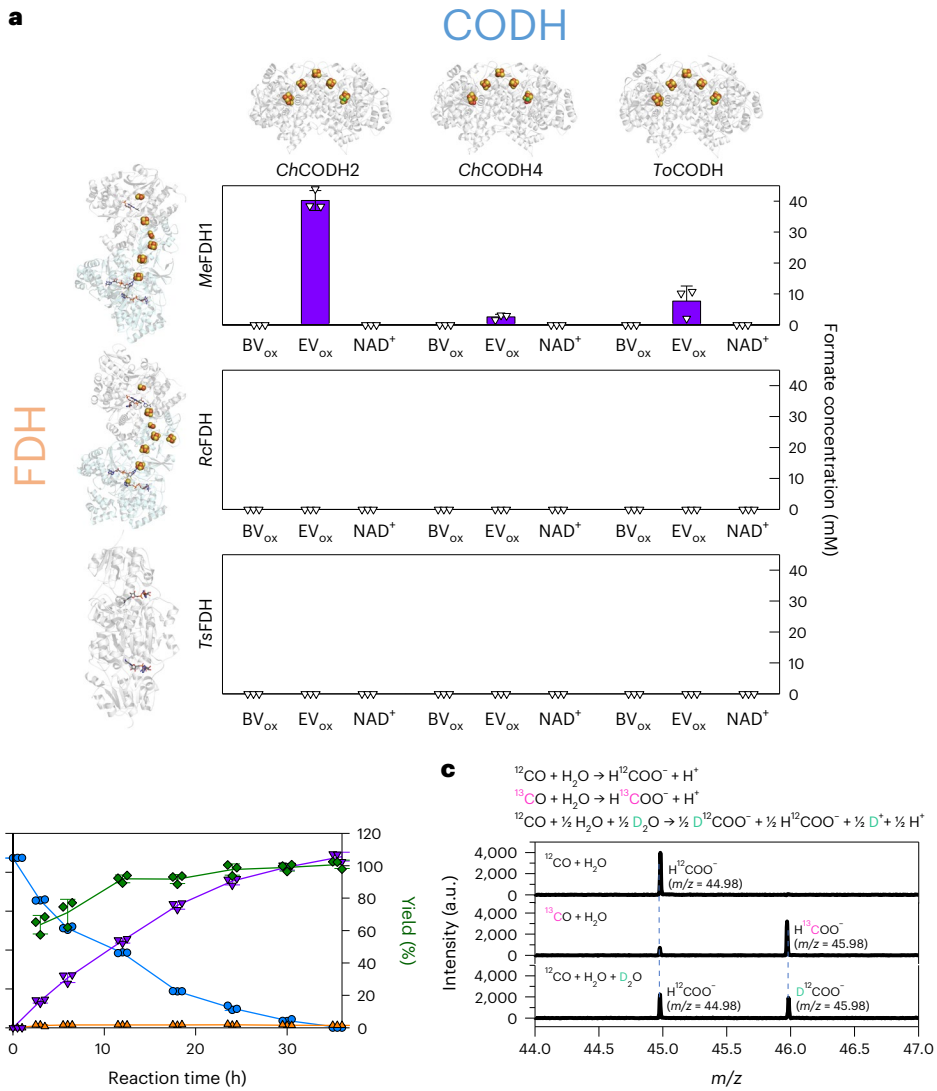

Fig. 2 | Examination and optimal conditions for enCOH. a, Selection of CODH and FDH for enCOH. *Ch*CODH2, *Ch*CODH4 and *To*CODH were the candidate CODHs, and *Me*FDH1, *Rc*FDH and *Ts*FDH were the candidate FDHs. Using BV_{ox}, EV_{ox} and NAD^+ as electron mediators, the formate (reverse triangles) productivity for each combination of CODHs and FDHs was determined over a 48 h period (data are presented as the mean ± s.d. of $n = 3$ replicates). **b**, Time course of the biotransformation through enCOH in a closed system. The percent of CO (circles) and CO_2 (triangles) was measured by GC and the formate (reverse triangles) amount was measured by HPLC over time. The yield (%, diamonds) of enCOH was calculated by dividing Δformate into ΔCO (data are presented as mean ± s.d. of $n = 3$ replicates). **c**, Tracking of enCOH using isotopes ^{13}CO and D_2O. ^{13}CO gas (magenta) and D_2O (cyan) were used for testing, and the molecular weight of the formate produced via enCOH was determined by mass spectrometry ($n = 1$ replicate). A total of 98.9% (vol/vol) of the carbon was ^{12}C and 99.9 % (vol/vol) of hydrogen was ^{1}H, leading most formate to have 45 g mol^{-1} of molar mass[18,19].

Table 4). Furthermore, kinetic stability and oxygen sensitivity were addressed through immobilization and enzyme engineering[29,40].

In evaluating individual enzyme's efficiencies toward mediators, we measured each enzyme's catalytic properties with different mediators in a controlled environment (pH 6.5, 30 °C), as shown in Extended Data Table 1 and Supplementary Fig. 4. Among the three tested mediators, the CODHs displayed no activity for NAD^+, and the FDHs showed very low activity for reduced BV, suggesting that the overall reaction rate of enCOH using these mediators would be slow. In contrast, the use of EV enabled CO-oxidizing activity in all CODHs tested and high CO_2-reducing activities in two metalloenzyme FDHs (*Me*FDH1 and *Rc*FDH), suggesting that EV is the most effective mediator. When using EV as an electron mediator, the highest CO-oxidizing and CO_2-reducing activities were observed with *Ch*CODH2 (290 U mg^{-1} using EV_{ox} as the electron acceptor) and *Me*FDH1 (66 U mg^{-1} using EV_{red} as the electron donor), respectively, among the six candidate enzymes.

To confirm the functionality of our proposed enCOH system involving CODH and FDH and to select a suitable enzyme combination set through experiments, we compared formate production with three commercially available mediators in their oxidized forms (BV_{ox}, EV_{ox} and NAD^+) due to their ease of handling compared with MV. Upon conducting reactions with 99.998% CO (vol/vol), we observed formate production for 48 h only when using mediator EV and *Me*FDH1 (Fig. 2a). Interestingly, the highest formate production was observed in the following order for CODH: *Ch*CODH2 (40.2 mM), *To*CODH (7.7 mM) and *Ch*CODH4 (2.6 mM), when combined with *Me*FDH1. *Rc*FDH devoid of the stabilizer KNO_3, as well as *Ts*FDH lacking metal in the active site, showed no formate production in any combination with CODHs and mediators. Accordingly, the combined activities of enzymes in the enCOH system synergistically led to high formate production. These findings suggest that *Ch*CODH2 and *Me*FDH1 are the best-performing set among the tested enzymes for enCOH.

https://doi.org/10.1038/s44286-024-00063-z

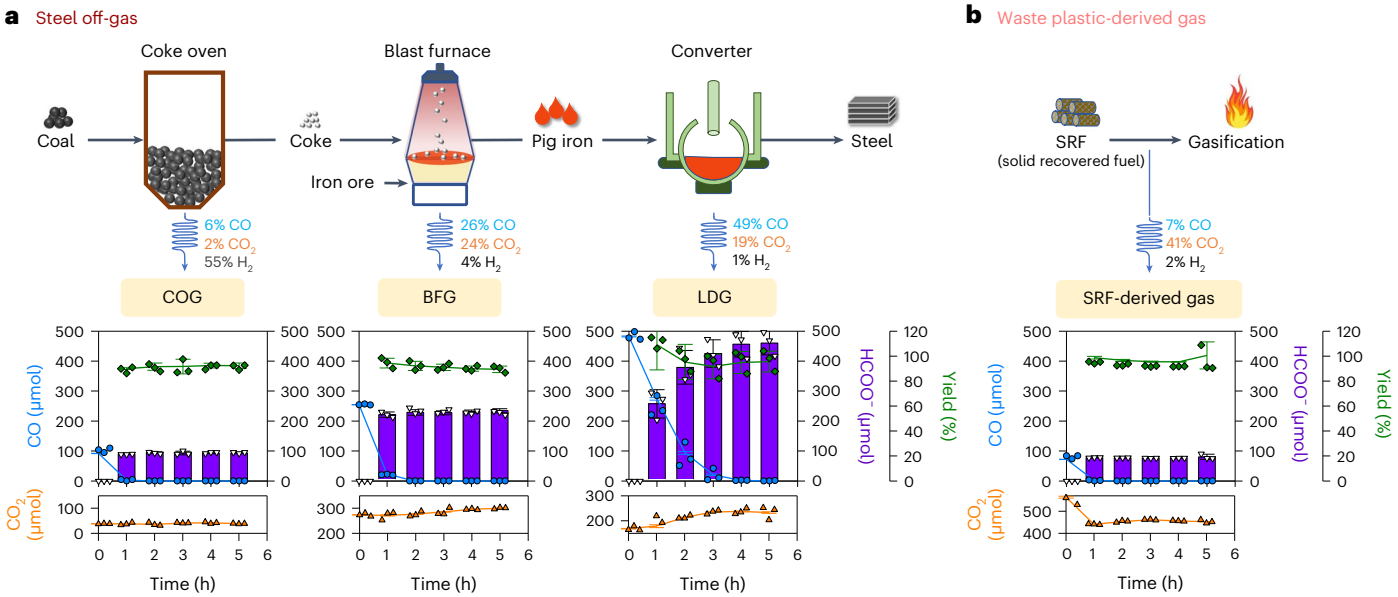

Fig. 3 | Efficient formate production with enCOH using real flue gas in a closed system. a, Influence of using real flue gas (BFG, COG, LDG) with enCOH. Industrial flue gases were used in enCOH. CO consumption (circles), CO_2 (triangles) and formate (inverse triangles) production, as well as yield (%, diamonds) were measured over time (data are presented as the mean ± s.d. of $n = 3$ replicates). **b**, Influence of using plastic-derived gas on enCOH. The gas derived from SRF gasification was used in enCOH. CO, CO_2 and formate were observed (data are presented as the mean ± s.d. of $n = 3$ replicates). The icon for gasification was made by Freepik from Flaticon (www.flaticon.com).

A more in-depth examination of the yield and selectivity of the reaction involving *Ch*CODH2 and *Me*FDH1 was carried out by conducting enzymatic conversion of the gas substrate CO to formate in closed serum bottles (Fig. 2b). The amounts of CO, CO_2 and formate were measured for 36 h in a closed system to estimate the yield of CO to formate. We observed that the formate gradually increased as CO was consumed, and, after 30 h, all the CO had been converted to formate. In the initial 12 h of the reaction, the formate production exhibited a slightly lower yield until the CO_2 accumulated to the level of ~1 mM. This can probably be attributed to *Me*FDH1's modest CO_2 affinity, at 3.9 mM (Supplementary Table 4). However, approaching the end point of the reaction, the consumed amount of CO was completely matched by the amount of produced formate, suggesting stoichiometric conversion between CO and formate (Fig. 2b and Supplementary Fig. 5). To verify whether the enzymatic reaction products of enCOH were genuinely a result of CO combining with water to generate formic acid, we examined the substrate and product masses using isotopes (^{13}CO). Our isotopic labeling experiments confirmed that the $HCOO^-$ was derived from ^{13}CO and D_2O (Fig. 2c). The molar mass of $H^{13}COO^-$ was found to be 45.98 g mol^{-1}, comparable to that of the $H^{12}COO^-$ (44.98 g mol^{-1}) obtained from $^{12}CO/H_2O$ conditions. Similarly, the H_2O/D_2O experiment with the same ratio showed a molar mass of $D^{12}COO^-$ of 45.98 g mol^{-1}. These results demonstrate that the carbon and hydrogen atoms of formate originated from the CO and water, respectively.

enCOH conversion of industrial off-gases to formate

An efficient enCOH system requires the simultaneous catalysis of CO and CO_2 substrates by the CODH and FDH enzymes, with both performing optimally. To achieve this, factors such as substrate and product inhibition, physicochemical conditions like pH, temperature and buffer, as well as the enzyme ratio, should be considered[41]. Interestingly, no inhibitory crosstalk was observed between the formate product on *Ch*CODH2 and the CO substrate on *Me*FDH1 (Supplementary Fig. 6). This is probably due to the tungsten-containing active site of FDH being tolerant to CO[42] and the size of formate hindering its passage through the substrate tunnel to access the nickel-containing active site of CODH (Supplementary Fig. 7). In addition to the inhibition effect, the pH profile revealed that both enzymes were active between pH 6.5 and 8, as shown in Supplementary Fig. 8a. A pH of 6.5 was chosen for enCOH because the overall reaction rate was governed by the enzymatic reaction of *Me*FDH1, which exhibited lower activity compared to *Ch*CODH2 (Extended Data Table 1). In terms of temperature, the enzyme activity progressively increased within the 20–70 °C range. However, based on kinetic stability, activity was better maintained at temperatures below 30 °C (Supplementary Fig. 8b–d), suggesting a trade-off between activity and stability.

The optimal temperature range for cost-effective and sustainable enzyme use would be at a temperature where there is a balance between maintaining a reasonable level of enzyme activity and ensuring their stability for long-term use. For example, higher temperatures may offer greater initial activity but at the expense of reduced enzyme stability, leading to frequent replacement or maintenance costs. By contrast, lower temperatures may yield slightly less activity but with greater stability and longevity, reducing overall operational costs. Long term, therefore, it is deemed more cost-effective to sustain consistent activity at lower temperatures rather than having high activity at elevated temperatures. The impact of various buffers (sodium phosphate, bis-tris propane, imidazole and MOPS (3-(*N*-morpholino) propanesulfonic acid)) at 50 mM concentrations appeared minimal, but sodium phosphate buffer emerged as the most effective (Supplementary Fig. 8e). Sodium phosphate, due to its affordability and availability compared to MOPS and other buffers like bis-tris propane and imidazole, offers a cost-effective, easier to source and practical solution for process scale-up. This choice effectively aligns enzyme performance with the economic considerations essential for industrial use and commercialization. Furthermore, a higher enzyme ratio of *Ch*CODH2 to FDH was shown to be beneficial, because a higher EV_{red}/EV_{ox} ratio is preferred for CO_2 reduction catalyzed by FDH (Supplementary Fig. 8f). Based on these findings, we concluded that both enzymes—*Ch*CODH2 and *Me*FDH1—can function effectively together under ambient/neutral conditions.

In steel-mill flue-gas applications, it is essential for the two enCOH enzymes to be tolerant to potential inhibitors such as O_2, HCN

https://doi.org/10.1038/s44286-024-00063-z

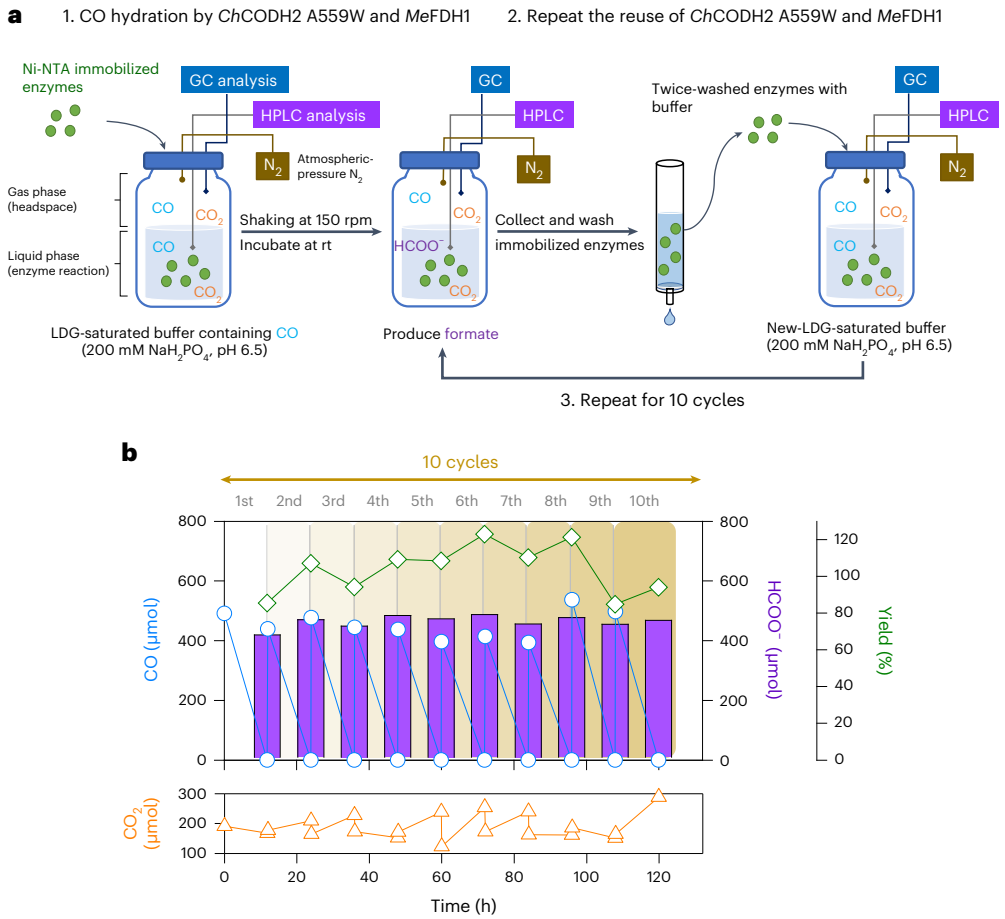

Fig. 4 | Enzymatic reusability for enCOH with LDG. a, Schematic of the experimental procedure. Enzymes with a His_6-tag were immobilized on Ni-NTA resin for ten cycles of reuse, with no severe loss in conversion rate. The reaction was performed at room temperature (rt) using a rubber-sealed serum bottle (115 ml) with LDG-purged reaction buffer (20 mM EV_{ox}, 200 mM sodium phosphate buffer pH 6.5 with purged LDG gas for 1 h). The immobilized enzyme was subsequently recovered through a disposable open column, washed twice with 200 mM sodium phosphate buffer pH 6.5 and reused after each reaction. **b**, Repeated reuse of enzymes for enCOH with LDG. By using CODH and FDH, immobilized on Ni-NTA agarose beads, the reusability of the enzymes was tested. CO (circles) consumption, CO_2 (triangles) and formate (reverse triangles) production, and yield (%, diamonds) were measured every 12 h ($n = 1$ replicate). Shaded bands denote the ten cycles.

(0.3–1.5 g N^{-1} m^{-3}) and SO_x (0.1–0.8 g N^{-1} m^{-3}), which are present in the flue gas of steel mills[43]. As shown in Supplementary Table 5, these gases exhibit variable oxygen concentrations (0–17%, vol/vol), necessitating the consideration of oxygen tolerance in industrial enzyme applications. For O_2, this challenge can be addressed by employing the recently developed O_2-tolerant *Ch*CODH2 A559W[29,44] and the well-established O_2-tolerant *Me*FDH1[23]. Apart from this, when examining the inhibitory effect, both *Ch*CODH2 and *Me*FDH1 retained their activities at aqueous cyanide and bisulfite concentrations corresponding to the range found in real flue gas (~0.05 μM cyanide; ~4 μM bisulfite). However, those enzyme activities declined when exposed to excessively high levels of cyanide and bisulfite, with half-maximal inhibitory concentration (IC_{50}) values of 2 μM for *Ch*CODH2 and 600 μM for *Me*FDH1 towards cyanide. FDH activity fully recovered post-inhibition, unlike the limited restoration of CODH. Such levels are typically not observed in steel-mill flue gases, which contain far lower concentrations (Supplementary Fig. 2). *Ch*CODH2 undergoes competitive inhibition by cyanide due to the binding of cyanide to the Ni atom of the catalytic center (Ni-Fe-S cluster), whereas *Me*FDH1 exhibits greater tolerance to cyanide[19]. No definitive inhibition mechanism caused by bisulfite on the two enzymes has been identified, and resistance to bisulfite is considerably higher than that of cyanide.

Leveraging this resilience, the production of formate using an O_2-tolerant enzyme-based enCOH (*Ch*CODH2 A559W and *Me*FDH1)[23,29] was evaluated in a closed reactor using real flue gas. Three representative waste gases, including coke-oven gas (COG), blast-furnace gas (BFG) and Linz–Donawitz gas (LDG), bottled gases from a Hyundai steel mill in Korea (Supplementary Table 5) and waste gas from mixed plastics (solid recovered fuel (SRF)) from the gasifier of Korea Institute of Energy Research (KIER) were used for the enCOH reaction (Fig. 3a and Supplementary Table 6). A mass-balance analysis for CO consumption and formate production was conducted by measuring CO levels in the gas phase and formate concentrations in the aqueous phase. Despite variations in the CO content and complex gas compositions of the supplied gases, all CO molecules were converted to formate, corroborating the theoretical yield of the enCOH reaction. As expected, LDG with higher carbon content produced a higher absolute amount of formate (~460 μmol) relative to the CO input, and COG with the lowest carbon content resulted in less formate (~93 μmol). Interestingly, COG, BFG, LDG and SRF-derived gas all achieved 100% conversion yields. This observation supports that an inexpensive LDG is a suitable waste gas for conversion into fuels and chemicals, due to the high content of recyclable CO/CO_2. Based on the gas composition of CO/CO_2, we classified waste real gas into three categories: COG/BFG, equivalent ratios; LDG, high CO/low CO_2; SRF-derived gas, low CO/high CO_2. As shown in Fig. 3b, enCOH transformed the low CO content in waste-plastic-derived gas into formate. These findings demonstrate that enCOH can effectively utilize CO across diverse gas compositions

https://doi.org/10.1038/s44286-024-00063-z

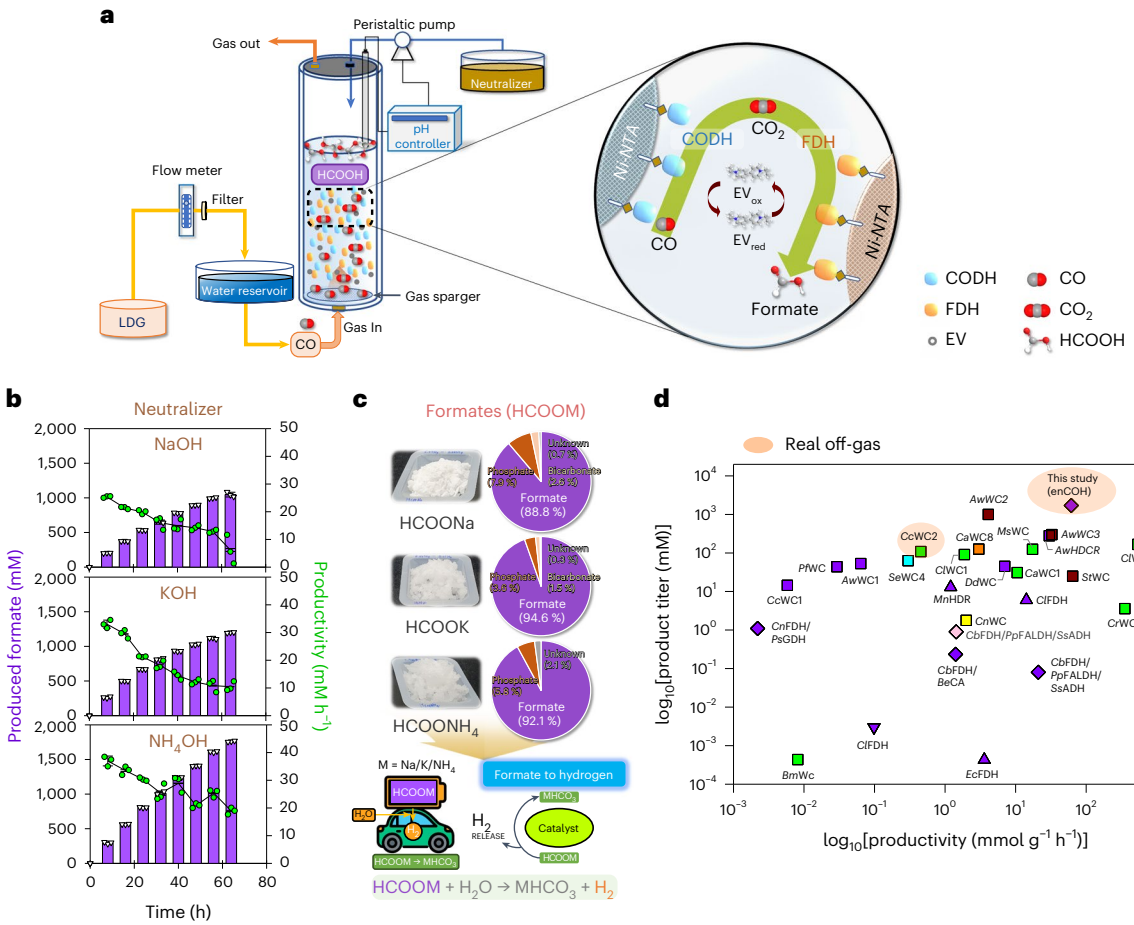

Fig. 5 | Formate production through enCOH with continuous gas flow. a, Long-term operation with continuous gas purging (LDG) and pH control in a 100-ml-scale reactor using various types of pH neutralizer. The 3D structures (CO, CO_2, formate and EV) were obtained from PubChem (https://pubchem.ncbi.nlm.nih.gov). **b**, The enCOH produced formate in the continuous gas flow system using NaOH, KOH or NH_4OH as the pH neutralizer (data are presented as the mean ± s.d. of $n = 3$ replicates). **c**, Extraction of three formate salts in a 100 ml reactor. The produced formate was purified to sodium, potassium or ammonium formate powder. In hydrogen production, formate salts undergo dehydrogenation, releasing hydrogen and transforming into bicarbonate. The icon was made by Freepik from Flaticon (www.flaticon.com). **d**, Feasibility evaluation of the biocatalytic system for formate production when utilizing synthetic gases or industrial off-gases. In commercial-scale operations, LanzaTech's ethanol production reaches up to 10 g l^{-1} h^{-1}. Due to the limited available details on catalyst usage and titer, direct comparisons are challenging. Nonetheless, this system's ethanol productivity is recognized as commercially viable.

because of its high substrate affinity for CO[29]. COG, BFG, LDG and SRF-derived gas have various compositions of gaseous components other than CO/CO_2, but these had no significant adverse effects on the enzymatic conversion of enCOH. For example, COG has a high H_2 content[29,45], but this had no impact (Fig. 3a–b and Supplementary Fig. 9). Based on this, it is expected that enCOH can utilize real waste gas with various compositions.

To achieve cost-effective enzymatic formate production, the activity of enCOH enzymes must be stably maintained during the conversion of CO to formate when LDG gas with higher CO/CO_2 is applied for long-term operation. A repeated reuse experiment was conducted, immobilizing CODH and FDH on nickel–nitrilotriacetic acid (Ni-NTA) resin (Fig. 4a,b). Consequently, formate productivity was sustained without sacrificing enzyme activity for over ten reuse cycles. This suggests that stable chemical production is attainable through enCOH using real flue gas due to the enzymes' resilience to toxic inhibitors such as cyanide and bisulfite.

Scaling-up enCOH for steel-mill field implementation

To explore the applicability of the enCOH system for continuous-flow reactions, a customized 100-ml enzyme reactor was designed and tested (Fig. 5a and Supplementary Fig. 10). Because formic acid production led to a continuous pH drop due to the low pK_a value (pK_a = 3.745), a neutralizing agent was required to keep the pH constant. We operated a 100-ml-scale reactor for enCOH under pH 6.5 control by continuously purging LDG, and evaluated the productivity and efficiency of the enCOH reaction using three representative neutralizers: NaOH, KOH and NH_4OH (Fig. 5b). For all the neutralizers, formate production remained stable for 64 h, yielding ~1.1 M (for NaOH), 1.2 M (for KOH) or 1.8 M (for NH_4OH). The resulting formate salts—sodium (HCOONa, 88.8% purity), potassium (HCOOK, 94.6% purity) and ammonium ($HCOONH_4$, 92.1% purity)—were easily obtained (Fig. 5c and Supplementary Fig. 11). Throughout this process, the use of NH_4OH not only yielded high productivity, but also generated ammonium formate, a notable compound that is challenging to produce via conventional industrial processes[46,47] and is synthesized easily through enzymatic reactions. Applying a catalyst to formate salts is anticipated to facilitate efficient hydrogen production, positioning them as promising hydrogen carriers[48], because formate salts are more eco-friendly and safe than formic acid, offering zero CO_2 emissions, reversible reactions, favorable thermodynamics and stable storage with fewer requirements.

To evaluate the biocatalytic efficiency of the enCOH system, we compared it with recent bioconversion technologies employed for

https://doi.org/10.1038/s44286-024-00063-z

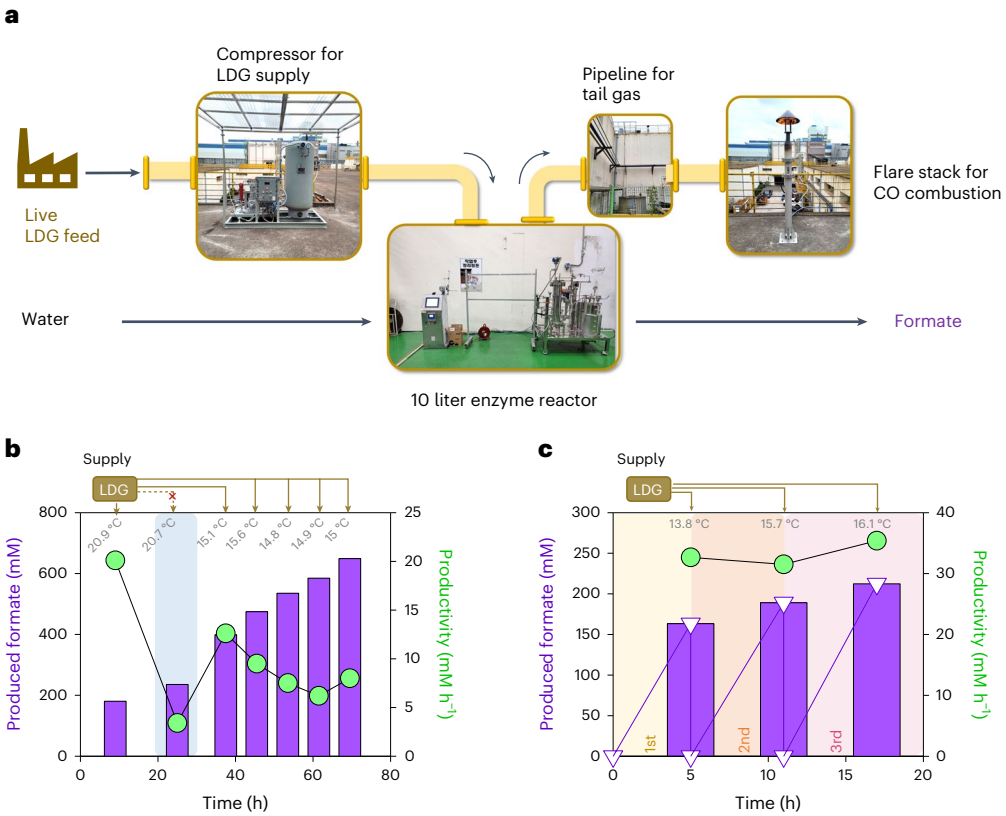

Fig. 6 | Field operation of the 10-l enCOH reactor with live off-gas. a, A scheme of the 10-l enzyme reactor (with a continuous feed of live LDG). enCOH was conducted in a continuous gas flow and pH-controlled system with immobilized enzymes in a large-scale reactor. **b**, Field operation of the enCOH reactor (10 l) at Hyundai Steel, with a continuous live LDG feed ($n = 1$ replicate). **c**, Repeated reuse of the enCOH biocatalyst for three cycles ($n = 1$ replicate). Shaded bands indicate the three cycles.

generating value-added products from CO_x gaseous sources (Fig. 5d and Supplementary Table 7). The enCOH system enables the production of high formate concentrations and notable productivity even using real flue gas; however, there are few reported works involving testing with real off-gases. In the context of production performance, the enCOH system demonstrates the following: (1) unlike whole-cell catalysis, this in vitro enzymatic system effectively overcomes challenges such as cell disruption and by-product formation by means of a combination of efficient enzymes, thus achieving high titers, and (2) leveraging CODH and FDH coupling, this system attains high productivity without external energy, distinguishing it from methods such as electrocatalysis and photocatalysis. This shows the in vitro enzyme system's ability to simultaneously achieve high titer and productivity, making it a competitive and viable option for industrial-scale production. This highlights the potential utility of the enCOH system for industrial applications.

Finally, a scaled-up 10-l reactor was designed for field operation of the enCOH reaction (Fig. 6a and Supplementary Fig. 12). The pilot reactor was installed to utilize a live feed of LDG directly connected from Hyundai Steel's site (Dangjin, Korea), without energy input. We observed that ~298.5 g of formate was produced during the 69.5-h enCOH reaction under ambient conditions (Fig. 6b). We also demonstrated repeated reuse of the enCOH biocatalysts (Fig. 6c). Unexpectedly, a temporary gas-supply interruption (at 25 h) and low temperature in the actual field environment negatively affected formate productivity (an electric temperature-control system could not be installed due to the strict safety regulations at the steel mill). Nonetheless, the enCOH system's stress test results indicate that actual waste by-product gas can be effectively used to produce the valuable chemical formate. Given the system's minimal susceptibility to variations in the CO content, catalytic inhibitors and gas composition, the enCOH reaction is a promising way to transform real flue gas into valuable products in industrial applications.

Discussion

Our technology facilitates the transformation of flue CO into formate at a near two-molar scale, demonstrating enzyme engineering's potent role in the crafting of practical industrial biocatalysts. Formate, being a versatile precursor, is increasingly a target in CO_2 reduction, chemical synthesis and energy production[12,49,50]. For green hydrogen, formate provides safe liquid storage[49]. We can explore ethyl/methyl formate and its use as a carbon source for chemicals such as polyhydroxyalkanoates[45], using natural and metabolic engineered strains[50]. Its versatility positions formate as a key player in reducing environmental footprints and advancing sustainable practices across industries. This oxygen-tolerant enzymatic technology[29,40] has shown potential for efficient mixed-waste gas conversion into valuable formate, advancing industrial CO_2 reduction and sustainable hydrogen carrier production.

In the pilot experiments, we connected directly to a live feed of LDG at Hyundai Steel, providing a realistic simulation of steel-mill conditions. This approach revealed how the enCOH system might perform in actual industrial settings. The live feed set-up brought unique operational challenges, such as stringent electricity usage constraints. Importantly, using a live LDG feed allowed us to examine the interactions of enzymes with potential contaminants as well as the reaction consistency, offering critical insights for practical application. The implementation of a 10-l-scale enzyme reactor at a steel company is an important step forward, demonstrating its potential for scalability and integration into industrial processes. Major steel companies in South Korea (POSCO and Hyundai Steel) are now exploring

opportunities for incorporating this technology into their processes. This not only emphasizes the versatility and applicability of enzyme engineering but also its potential to promote sustainability within industrial processes[20,24].

In conclusion, the enzymatic molar-scale production of formate from complex industrial off-gases using a rationally designed in vitro reaction is a notable stride towards sustainable energy production systems and the realm of industrial biotechnology. The potential ramifications of this technology are considerable, providing invaluable insights for scientific, environmental and industrial sectors seeking to reduce greenhouse-gas emissions and support sustainable industrial processes.

Methods

Gene synthesis and cloning for expression

All the *Ch*CODH2 (UniProt accession number Q9F8A8) and *Ch*CODH4 (Q9F8A8) genes from *C. hydrogenoformans*[29] were synthesized by Macrogen (Korea), optimized for *Nde*I and *Bam*HI restriction sites, and cloned into pET-28a(+) (Novagen), which encodes an N-terminal His-tag. These constructs were then transformed into *E. coli* BL21 harboring pRKISC[51] for expression. The tungsten-based *Me*FDH1 genes, fdh1A (C5ATT7) and fdh1B (C5ATT6), were integrated into pCM110 and expressed in *M. extorquens* AM1[34], because expression in *E. coli* was unsuccessful. The molybdenum-based *Rc*FDH genes (fdhABC, D5AQH0–2; fdhE, D5AQG8) from *R. capsulatus*[35,36] were designed for *Nhe*I and *Sac*I restriction sites, cloned into pTrcHis A, and expressed in *E. coli* MC1061. The non-metallic *Ts*FDH gene (Q76EB7) from *Thiobacillus* sp. KNK65MA, optimized for *Nhe*I and *EcoR*I restriction sites, was integrated into pUC57 and expressed in *E. coli* BL21[37]. Finally, the *To*CODH gene (B6YWP3) from *T. onnurineus* NA1 was optimized for *Nco*I and *Not*I restriction sites, synthesized, and confirmed by sequence verification prior to cloning[33]. The related gene, plasmid and host details are provided in Supplementary Table 8.

Enzyme expression and purification

Except for *Me*FDH1, the enzymes utilized in this study were acquired via heterologous expression in *E. coli*. All enzymes were isolated using Ni-NTA agarose beads to purify His_6-tagged proteins under anaerobic conditions. The expression and purification process, primarily focusing on the enCOH enzymes *Ch*CODH2 and *Me*FDH1, is described here, aligning with methods reported in previous research[29,30,33–37].

Escherichia coli cultures expressing *Ch*CODH2, *Ch*CODH4 and *To*CODH were grown in modified terrific broth medium supplemented with 0.02 mM $NiCl_2$, 0.1 mM $FeSO_4$, 2 mM L-cysteine and antibiotics (kanamycin 50 μg ml^{-1}, tetracycline 10 μg ml^{-1}), at 37 °C and 200 rpm. Upon reaching an optical density at 600 nm (OD_{600}) of between 0.4 and 0.6, overexpression of CODH was induced with 0.2 mM isopropyl β-D-1-thiogalactopyranoside (IPTG), 0.5 mM $NiCl_2$, 1 mM $FeSO_4$ and 50 mM KNO_3, after 1 h of N_2 flushing at 30 °C. For *Me*FDH1 expression[52], the defined medium with 16 g l^{-1} succinate as a carbon source and 9.9 mg l^{-1} Na_2WO_4 was used, with *M. extorquens* AM1, at 30 °C and 200 r.p.m. At OD_{600} 0.4–0.6, 0.5% (vol/vol) methanol was added for induction. *Rc*FDH and *Ts*FDH were expressed in LB medium under conditions aligning with reported methodologies[36,37]. *Rc*FDH expression required 150 μg ml^{-1} ampicillin, 1 mM sodium molybdate and 20 μM IPTG, incubated at 30 °C with 130 rpm agitation. *Ts*FDH expression employed 50 μg ml^{-1} ampicillin and 1 mM IPTG, incubated at 37 °C and agitated at 200 rpm.

For kinetic analysis, cells were lysed either by sonication in an anaerobic chamber (COY Laboratory Products) or by a homogenizer (GEA Mechanical Equipment) for larger enCOH reaction preparations (100 ml reactor). The lysis buffers varied depending on the enzyme: CODH-expressing cells utilized a 50 mM sodium phosphate buffer (pH 8.0) of 300 mM NaCl, 2 mM dithioerythritol (DTE) and 2 μM resazurin; FDH-expressing cells employed a 50 mM MOPS (3-(*N*-morpholino)propanesulfonic acid) buffer (pH 7.0) containing 300 mM NaCl, 2 mM DTE and 2 μM resazurin. After lysis, the supernatant from the centrifugation (14,000*g*, 4 °C, 20 min) was mixed with Ni-NTA agarose beads and incubated for 15 min in an anaerobic chamber. The enzyme-bound beads were washed and directly used for enCOH reactions or eluted for further assays. The elution buffers were similar to the lysis buffers but contained 20–250 mM imidazole for CODH and 20–300 mM imidazole for FDH. An additional 10 mM KNO_3 was used for *Rc*FDH purification.

Enzyme activity measurement

For the CODH activity assay, a 200 mM sodium phosphate reaction buffer (pH 6.5) containing 20 mM oxidized mediators (BV_{ox}; EV_{ox}; NAD^+) and 2 mM DTE was saturated with 99.998% (vol/vol) CO gas (Air Liquide Korea). The reaction was initiated with 0.1 μg of enzyme, and the activity was estimated at 30 °C by spectrophotometrically monitoring the initial rate of absorbance increase at appropriate wavelengths for each reduced mediator (BV_{red}, ε_{578} = 9,750 M^{-1} cm^{-1}; EV_{red}, ε_{546} = 10,000 M^{-1} cm^{-1}; NADH, ε_{340} = 6,220 M^{-1} cm^{-1})[29,30,53].

For the FDH activity assay, the reaction was initiated by adding 1 μg of enzyme to a 200 mM sodium phosphate buffer (pH 6.5) containing 100 mM sodium bicarbonate, 0.1 mM reduced mediators (BV_{red}, EV_{red}, NADH) and 2 mM DTE at 30 °C. Activity was estimated by tracking the initial rate of decline in absorbance for each reduced mediator spectrophotometrically. Reduced viologens, BV_{red} and EV_{red}, were prepared anaerobically by mixing 200 mM oxidized viologens with 1 g of zinc and filtering through a 0.45-μm syringe filter[54]. All experiments were performed in triplicate.

Enzyme catalytic properties

Kinetic analysis of enzyme activity was performed using varying concentrations of electron mediators (0.5–8 mM for CODH-mediated CO oxidation and 0.006–0.1 mM for FDH-mediated CO_2 reduction) in conditions identical to the activity assays. The kinetic parameters for BV, EV and NAD(H) were determined using Hanes–Woolf plots. Enzyme activity profiles across different pH values (6–8) and temperatures (20–70 °C) were assessed using pH-adjusted buffers and 200 mM sodium phosphate buffer (pH 6.5), respectively.

Inhibition of CODH activity by formate was evaluated using a CO-saturated sodium phosphate buffer (pH 6.5) with 20 mM EV_{ox}, 2 mM DTE, 2 μM resazurin and varying formate concentrations (0–1 M). The inhibitory effect of CO on FDH activity was assayed in a sodium phosphate buffer (pH 6.5) supplemented with 100 mM sodium bicarbonate, 0.1 mM EV_{red}, 2 mM DTE, 2 μM resazurin and different CO concentrations (0–1 mM). According to Henry's law, a 99.998% (vol/vol) CO purged buffer at room temperature and pressure contains ~1 mM CO. To assess enzyme inhibition by KCN and $NaHSO_3$, the enzymes (4 μg) were anaerobically incubated with varying concentrations of inhibitors (10 nM–20 mM) for 30 min in sodium phosphate buffer (pH 6.5). The residual enzyme activities were subsequently measured. In the recovery experiments for enzymes against KCN and sodium bisulfite inhibitors, Ni-NTA-immobilized CODH and FDH were treated with 10 mM inhibitors in a time-course experiment spanning 2 h. After the treatment period, the enzymes were washed twice with 50 mM bis-tris-propane buffer (pH 6.5). Residual activity was subsequently measured over time using 20 mM EV_{ox} for CO oxidation and 0.1 mM EV_{red} for CO_2 reduction. All experiments were performed in triplicate.

High-performance liquid chromatography and gas chromatography analysis

In this study, formate (reaction product) was analyzed using high-performance liquid chromatography (HPLC), and the gaseous components, including CO (substrate), CO_2 (intermediate) and other gases such as H_2 and N_2, were quantified via gas chromatography (GC) to monitor their changes during the enzymatic reactions. Immediately after

sampling, formate from the enCOH reaction solution was quenched using a 6 M H_2SO_4 solution in a 10:1 ratio. HPLC measurements utilized an Aminex HPX-87H column (Bio-Rad) and an RID-20A refractive index detector (Shimadzu) (mobile phase, 5 mM H_2SO_4; flow rate, 0.6 ml min^{-1}).

The gas content in the headspace of the serum bottle from enCOH experiments was analyzed using a 7890B GC-TCD system (Agilent Technologies). A 0.5-ml gas sample was obtained using a gas-tight syringe (Trajan Scientific and Medical). GC analyses employed a Carboxen-1000 column (Supelco) with argon as the carrier gas (flow rate, 30 ml min^{-1}). The oven temperature was initially set at 35 °C for 5 min, and then ramped to 225 °C at a rate of 20 °C min^{-1}. All experiments were performed in triplicate.

Electrospray ionization mass spectrometry, Fourier-transform infrared spectroscopy and NMR analysis

The isotopic identity of enCOH products was confirmed using electrospray ionization mass spectrometry (ESI-MS). Reaction mixtures, prepared with ^{13}CO (99% atom ^{13}C, Cambridge Isotope Laboratories) or D_2O (99.9% atom D, Sigma-Aldrich), yielded formates with distinct masses. Either ^{12}CO or ^{13}CO was introduced into a reaction buffer (10 mM EV_{ox}, 2 mM DTE, 2 µM resazurin; for D_2O experiments, up to 50% (vol/vol) D_2O) in a serum bottle. Reactions were initiated by injecting 2,000 U *Ch*CODH2 and 20 U *Me*FDH1, and quenched after 24 h with 10 M KOH for ESI-MS analysis. The ESI-MS set-up (JMS-T100LP, JEOL) was operated in negative mode, with a needle voltage of −2,000 V, a 250 °C desolvation chamber, −30 V and 80 °C orifice 1, −5 V ring lens, −10 V orifice 2 and 100 V ion guide RF. A survey time-of-flight MS experiment scanned m/z from 10 to 100 for isotope-labeled formate.

To characterize the formate salts produced from enCOH reactions, Fourier-transform infrared spectroscopy (FT-IR) and NMR were used. For three formate salts (sodium, potassium and ammonium) analysis, FT-IR was used. Those salts were produced with immobilized enzymes (35 U of Ni-NTA immobilized *Ch*CODH2 A559W and 125 U of Ni-NTA *Me*FDH1) in reaction buffer with 10 mM EV_{ox}, 2 mM DTE and 2 µM resazurin. FT-IR spectra were acquired on a Nicolet iS50 spectrometer (Thermo Fisher Scientific) in attenuated total reflection mode. ^1H-NMR spectra were acquired using a Bruker 400-MHz AVANCE III HD spectrometer at ambient temperature, with D_2O as the reference (D_2O, $\delta = 4.69$ ppm; formate, $\delta = 8.37$ ppm).

Evaluation of enCOH enzyme candidates

To identify the most effective enzymes for the enCOH reaction, combinations of various enzymes and electron mediators were examined. For CODHs, 100 µg each of *Ch*CODH2, *Ch*CODH4 and *To*CODH were tested. For FDHs, 250 µg each of *Me*FDH1, *Rc*FDH and *Ts*FDH were evaluated. Serum bottles containing a 200 mM bis-tris propane buffer (pH 6.5) supplemented with 10 mM electron mediators (BV_{ox}, EV_{ox} and NAD^+), 2 mM DTE and 2 µM resazurin were purged with 99.998% (vol/vol) CO gas for 1 h. Reactions at room temperature were initiated by enzyme injection, and formate concentration was measured after 48 h. For the time-course analysis, the conditions remained the same, employing *Ch*CODH2, *Me*FDH1 and EV_{ox}. The reaction was monitored over time using both HPLC and GC. All experiments were performed in triplicate.

Enzymatic reaction in sealed serum bottles

The enCOH reactions were performed at room temperature in 120-ml serum bottles (sealed with rubber) containing 200 mM sodium phosphate buffer (pH 6.5), 10 mM EV_{ox}, 2 mM DTE and 2 µM resazurin. The bottles were purged for 1 h with test gases (99.998% (vol/vol) CO or real flue gases, including COG, BFG, LDG or SRF-derived gas) to fill the headspace. COG, BFG and LDG (compressed to 4–5 MPa in 47-l cylinders) were sourced from Hyundai Steel[29,30], and SRF-derived gas (compressed to 9 bar in 10-l cylinders) were from the Korea Institute of Energy Research[30,55,56]. The reactions were initiated by injecting 35 U of *Ch*CODH2 A559W mutant and 125 U of *Me*FDH1, then the bottles were shaken at 150 rpm at room temperature. The pressure was equilibrated at each sampling by supplying N_2 gas (99.999%, vol/vol) to compensate for the gas molecule consumption. All experiments were performed in triplicate.

For repeated enzyme usage, enzymes immobilized on Ni-NTA agarose beads were employed. The reactions contained 200 mM sodium phosphate buffer (pH 6.5), 10 mM EV_{ox}, 2 mM DTE, 2 µM resazurin, 35 U of immobilized *Ch*CODH2 A559W mutant and 125 U of immobilized *Me*FDH1. Post-reaction beads were collected in a disposable column and washed twice with 20 ml of 200 mM sodium phosphate buffer (pH 6.5). LDG was supplied every 12 h after replenishing with fresh sodium phosphate buffer solution (pH 6.5) containing 10 mM EV_{ox}, 2 mM DTE and 2 µM resazurin.

Enzymatic reaction in the 100-ml bubble column reactor

To optimize gas substrate reactivity in the enzymatic reactions, we utilized a custom-designed 100-ml bubble-type column reactor, fabricated by newhillbiotech. This reactor is a four-necked glass cylinder with a bottom-up gas-supply system, a diameter of 29 mm and height of 563 mm.

The enCOH reactions were conducted at room temperature within this reactor, which was filled with 50 mM sodium phosphate buffer (pH 6.5), 10 mM EV, 2 mM DTE, 35 U of immobilized *Ch*CODH2 A559W mutant and 125 U of immobilized *Me*FDH1. The reactor was continuously supplied with real flue LDG (compressed to 4–5 MPa in a 47-l cylinder) at a rate of 100 ml min^{-1}, introduced via a sintered glass filter installed at the bottom of the reactor. To maintain a pH of 6.5 in each experiment set and generate distinct types of formate salt, we utilized neutralizers including 10 M solutions of NaOH, KOH and NH_4OH. All experiments were performed in triplicate.

10-l enzymatic reactor installation at Hyundai steel

A 15-l bubble column reactor (STS 316L; diameter, 16.5 cm; height, 80.6 cm) was customized and constructed by CNS Engineering. Key details of the reactor design are presented in Supplementary Fig. 12. The reactor was operated at Hyundai Steel using *Ch*CODH2 A559W and *Me*FDH1 proteins, expressed in a customized fermenter by culturing CODH-expressing *E. coli* and FDH-expressing *M. extorquens* cells. Summary data, including the total weight of cultured strains, the total amount of expressed proteins and protein activities, are provided in Supplementary Table 9 and Supplementary Fig. 13. For large-scale protein production, *Ch*CODH2 A559W and *Me*FDH1 were expressed under anaerobic and aerobic conditions, respectively. This process took place in 5-l (using the dual fermenter system MARADO-05D-PS) and 100-l (utilizing a customized pilot-scale fermentation system) fermenters, both constructed by CNS Engineering. A video demonstrating the set-up and operation of the reaction apparatus is provided in Supplementary Video 1. During operation, LDG from the steel mill was continuously supplied via a compressor (compressed to 3 bar) into the 15-l reactor, which held 10 l of 50 mM sodium phosphate solution (pH 6.5), supplemented with 1 mM EV_{ox}, 2 mM DTE, 3.5 kU of immobilized *Ch*CODH2 A559W and 12.5 kU of immobilized *Me*FDH1. The pH was maintained at 6.5 by adding 10 N NaOH as a neutralizing agent.

Salt formate separation

Following the 100-ml reactor operation, the solution was filtered through a sintered glass filter, followed by an activated carbon bed (10 g, Darco-G60, Sigma-Aldrich). The adsorptive properties of activated carbon enabled formate separation, based on the reported affinity of viologens for activated carbon[57,58]. The recovered solution was dried in a convection oven at 90 °C overnight to yield powdered solids. The purity and identity of the produced formate were verified using HPLC, FT-IR and NMR analyses, respectively (Supplementary Table 10).

Reporting summary

Further information on research design is available in the Nature Portfolio Reporting Summary linked to this Article.

Data availability

All data supporting the findings of this study are available within the article and the Supplementary Information. All source data have been deposited on figshare at https://doi.org/10.6084/m9.figshare.25433956.v2 (ref. 59). 3D chemical structures data for CO, CO_2, formate and ethyl viologen are available in the PubChem database (https://pubchem.ncbi.nlm.nih.gov/).

References

1. *Iron and Steel Technology Roadmap: Towards More Sustainable Steelmaking* (International Energy Agency, 2020). https://www.iea.org/reports/iron-and-steel-technology-roadmap
2. Kohse-Hoeinghaus, K. Combustion, chemistry and carbon neutrality. *Chem. Rev.* **123**, 5139–5219 (2023).
3. Yang, F., Meerman, J. C. & Faaij, A. P. C. Carbon capture and biomass in industry: a techno-economic analysis and comparison of negative emission options. *Renew. Sust. Energ. Rev.* **144**, 111028 (2021).
4. De Ras, K., Van de Vijver, R., Galvita, V. V., Marin, G. B. & Van Geem, K. M. Carbon capture and utilization in the steel industry: challenges and opportunities for chemical engineering. *Curr. Opin. Chem. Eng.* **26**, 81–87 (2019).
5. Sun, Y. Q. et al. Decarbonising the iron and steel sector for a 2 °C target using inherent waste streams. *Nat. Commun.* **13**, 297 (2022).
6. Wang, P. et al. Efficiency stagnation in global steel production urges joint supply- and demand-side mitigation efforts. *Nat. Commun.* **12**, 2066 (2021).
7. Khodakov, A. Y., Chu, W. & Fongarland, P. Advances in the development of novel cobalt Fischer–Tropsch catalysts for synthesis of long-chain hydrocarbons and clean fuels. *Chem. Rev.* **107**, 1692–1744 (2007).
8. Gokhale, A. A., Dumesic, J. A. & Mavrikakis, M. On the mechanism of low-temperature water gas shift reaction on copper. *J. Am. Chem. Soc.* **130**, 1402–1414 (2008).
9. Santos, V. P. et al. Metal organic framework-mediated synthesis of highly active and stable Fischer–Tropsch catalysts. *Nat. Commun.* **6**, 6451 (2015).
10. Liu, B. et al. CO_2 formation mechanism in Fischer–Tropsch synthesis over iron-based catalysts: a combined experimental and theoretical study. *Catal. Sci. Technol.* **8**, 5288–5301 (2018).
11. Köpke, M., Mihalcea, C., Bromley, J. C. & Simpson, S. D. Fermentative production of ethanol from carbon monoxide. *Curr. Opin. Biotechnol.* **22**, 320–325 (2011).
12. Schuchmann, K. & Muller, V. Direct and reversible hydrogenation of CO_2 to formate by a bacterial carbon dioxide reductase. *Science* **342**, 1382–1385 (2013).
13. Ljungdahl, L. G. & Wood, H. G. Total synthesis of acetate from CO_2 by heterotrophic bacteria. *Annu. Rev. Microbiol.* **23**, 515–538 (1969).
14. Ragsdale, S. W. & Pierce, E. Acetogenesis and the Wood-Ljungdahl pathway of CO_2 fixation. *Biochim. Biophys. Acta* **1784**, 1873–1898 (2008).
15. Fast, A. G. & Papoutsakis, E. T. Stoichiometric and energetic analyses of non-photosynthetic CO_2-fixation pathways to support synthetic biology strategies for production of fuels and chemicals. *Curr. Opin. Chem. Eng.* **1**, 380–395 (2012).
16. Martin, W. F., Sousa, F. L. & Lane, N. Energy at life's origin. *Science* **344**, 1092–1093 (2014).
17. Nisbet, E. G. & Sleep, N. H. The habitat and nature of early life. *Nature* **409**, 1083–1091 (2001).
18. Jeoung, J. H. & Dobbek, H. Structural basis of cyanide inhibition of Ni, Fe-containing carbon monoxide dehydrogenase. *J. Am. Chem. Soc.* **131**, 9922–9923 (2009).
19. Ha, S. W. et al. Interaction of potassium cyanide with the [Ni–4Fe–5S] active site cluster of CO dehydrogenase from *Carboxydothermus hydrogenoformans*. *J. Biol. Chem.* **282**, 10639–10646 (2007).
20. Can, M., Armstrong, F. A. & Ragsdale, S. W. Structure, function and mechanism of the nickel metalloenzymes, CO dehydrogenase and acetyl-CoA synthase. *Chem. Rev.* **114**, 4149–4174 (2014).
21. Rivas, M. G., Gonzalez, P. J., Brondino, C. D., Moura, J. J. G. & Moura, I. EPR characterization of the molybdenum(V) forms of formate dehydrogenase from *Desulfovibrio desulfuricans* ATCC 27774 upon formate reduction. *J. Inorg. Biochem.* **101**, 1617–1622 (2007).
22. Robinson, W. E., Bassegoda, A., Reisner, E. & Hirst, J. Oxidation-state-dependent binding properties of the active site in a Mo-containing formate dehydrogenase. *J. Am. Chem. Soc.* **139**, 9927–9936 (2017).
23. Laukel, M., Chistoserdova, L., Lidstrom, M. E. & Vorholt, J. A. The tungsten-containing formate dehydrogenase from *Methylobacterium extorquens* AM1: purification and properties. *Eur. J. Biochem.* **270**, 325–333 (2003).
24. Stripp, S. T. et al. Second and outer coordination sphere effects in nitrogenase, hydrogenase, formate dehydrogenase and CO dehydrogenase. *Chem. Rev.* **122**, 11900–11973 (2022).
25. Zhou, W. et al. New horizon in C1 chemistry: breaking the selectivity limitation in transformation of syngas and hydrogenation of CO_2 into hydrocarbon chemicals and fuels. *Chem. Soc. Rev.* **48**, 3193–3228 (2019).
26. Liew, F. et al. Gas fermentation—a flexible platform for commercial scale production of low-carbon-fuels and chemicals from waste and renewable feedstocks. *Front. Microbiol.* **7**, 694 (2016).
27. Anderson, M. E., Derose, V. J., Hoffman, B. M. & Lindahl, P. A. Identification of a cyanide binding-site in CO dehydrogenase from *Clostridium thermoaceticum* using EPR and ENDOR spectroscopies. *J. Am. Chem. Soc.* **115**, 12204–12205 (1993).
28. Shima, S. & Ataka, K. Isocyanides inhibit [Fe]-hydrogenase with very high affinity. *FEBS Lett.* **585**, 353–356 (2011).
29. Kim, S. M. et al. O_2-tolerant CO dehydrogenase via tunnel redesign for the removal of CO from industrial flue gas. *Nat. Catal.* **5**, 807–817 (2022).
30. Kim, S. M. et al. Identifying a key spot for electron mediator-interaction to tailor CO dehydrogenase's affinity. *Nat. Commun.* **15**, 2732 (2024).
31. Dobbek, H., Svetlitchnyi, V., Gremer, L., Huber, R. & Meyer, O. Crystal structure of a carbon monoxide dehydrogenase reveals a [Ni–4Fe–5S] cluster. *Science* **293**, 1281–1285 (2001).
32. Domnik, L. et al. CODH-IV: a high-efficiency CO-scavenging CO dehydrogenase with resistance to O_2. *Angew. Chem. Int. Ed.* **56**, 15466–15469 (2017).
33. Lee, S. H., Lee, S. M., Kang, S. G. & Lee, H. S. Enhanced H_2 production by deletion of the Tfx family DNA-binding protein in the hyperthermophilic archaeon *Thermococcus onnurineus* NA1. *Int. J. Hydrogen Energ.* **46**, 35189–35197 (2021).
34. Jang, J., Jeon, B. W. & Kim, Y. H. Bioelectrochemical conversion of CO_2 to value added product formate using engineered *Methylobacterium extorquens*. *Sci. Rep.* **8**, 7211 (2018).
35. Hartmann, T. & Leimkuhler, S. The oxygen-tolerant and NAD^+-dependent formate dehydrogenase from *Rhodobacter capsulatus* is able to catalyze the reduction of CO_2 to formate. *FEBS J.* **280**, 6083–6096 (2013).
36. Choi, E. G., Yeon, Y. J., Min, K. & Kim, Y. H. Communication—CO_2 reduction to formate: an electro-enzymatic approach using a formate dehydrogenase from *Rhodobacter capsulatus*. *J. Electrochem. Soc.* **165**, H446–H448 (2018).

37. Choe, H. et al. Efficient CO_2-reducing activity of NAD-dependent formate dehydrogenase from *Thiobacillus* sp KNK65MA for formate production from CO_2 gas. *PLoS One* **9**, e103111 (2014).
38. Benvenuti, M. et al. The two CO-dehydrogenases of *Thermococcus* sp. AM4. *BBA Bioenerg.* **1861**, 148188 (2020).
39. Leo, F., Schwarz, F. M., Schuchmann, K. & Müller, V. Capture of carbon dioxide and hydrogen by engineered *Escherichia coli*: hydrogen-dependent CO_2 reduction to formate. *Appl. Microbiol. Biotechnol.* **105**, 5861–5872 (2021).
40. Kim, S. M., Kang, S. H., Jeon, B. W. & Kim, Y. H. Tunnel engineering of gas-converting enzymes for inhibitor retardation and substrate acceleration. *Bioresour. Technol.* **394**, 130248 (2024).
41. Hold, C., Billerbeck, S. & Panke, S. Forward design of a complex enzyme cascade reaction. *Nat. Commun.* **7**, 12971 (2016).
42. Stewart, D. W. G. et al. The role of tungsten oxide in enhancing the carbon monoxide tolerance of platinum-based hydrogen oxidation catalysts. *ACS Appl. Mater. Interfaces* **12**, 37079–37091 (2020).
43. Caillat, S. Burners in the steel industry: utilization of by-product combustion gases in reheating furnaces and annealing lines. *Energy Procedia* **120**, 20–27 (2017).
44. An enzyme's new 'tunnels' boost its waste-grabbing prowess. *Nature* **609**, 657 (2022).
45. Hwang, H. W. et al. Two-stage bioconversion of carbon monoxide to biopolymers via formate as an intermediate. *Chem. Eng. J.* **389**, 124394 (2020).
46. Weissermel, K. & Arpe, H. *Industrial Organic Chemistry: Important Initial and Intermediate Products* (Wiley-VCH, 1976).
47. Liu, Q. et al. Towards a sustainable synthesis of formate salts: combined catalytic methanol dehydrogenation and bicarbonate hydrogenation. *Angew. Chem. Int. Ed.* **53**, 7085–7088 (2014).
48. Calabrese, M., Russo, D., di Benedetto, A., Marotta, R. & Andreozzi, R. Formate/bicarbonate interconversion for safe hydrogen storage: a review. *Renew. Sust. Energ. Rev.* **173**, 113102 (2023).
49. Eppinger, J. & Huang, K.-W. Formic acid as a hydrogen energy carrier. *ACS Energy Lett.* **2**, 188–195 (2017).
50. Yishai, O., Lindner, S. N., Gonzalez de la Cruz, J., Tenenboim, H. & Bar-Even, A. The formate bio-economy. *Curr. Opin. Chem. Biol.* **35**, 1–9 (2016).
51. Nakamura, M., Saeki, K. & Takahashi, Y. Hyperproduction of recombinant ferredoxins in *Escherichia coli* by coexpression of the ORF1-ORF2-*iscS-iscU-iscA-hscB-hscA-fdx*-ORF3 gene cluster. *J. Biochem.* **126**, 10–18 (1999).
52. Phan, U. T., Jeon, B. W. & Kim, Y. H. Microbial engineering of *Methylorubrumextorquens* AM1 to enhance CO_2 conversion into formate. *Enzyme Microb.Technol.* **168**, 110264 (2023).
53. Miller, E., Wohlfarth, G. & Diekert, G. Studies on tetrachloroethene respiration in *Dehalospirillum multivorans*. *Arch. Microbiol.* **166**, 379–387 (1996).
54. Moon, K., Grindstaff, J., Sobransingh, D. & Kaifer, A. E. Cueurbit[8] uril-mediated redox-controlled self-assembly of viologen-containing dendrimers. *Angew.Chem. Int. Ed.* **43**, 5496–5499 (2004).
55. Tokmurzin, D. et al. High temperature flash pyrolysis characteristics of waste plastics (SRF) in a bubbling fluidized bed: effect of temperature and pelletizing. *Fuel* **326**, 125022 (2022).
56. Tokmurzin, D. Three-dimensional CFD simulation of waste plastic (SRF) gasification in a bubbling fluidized bed with detailed kinetic chemical model. *Energy Convers. Manag.* **267**, 115925 (2022).
57. Hamadi, N. K., Swaminathan, S. & Chen, X. D. Adsorption of paraquat dichloride from aqueous solution by activated carbon derived from used tires. *J. Hazard. Mater.* **112**, 133–141 (2004).
58. Nakamura, T. et al. Adsorption removal of paraquat and diquat onto activated carbon at different adsorption temperature. *Toxicol. Environ. Chem.* **70**, 275–280 (1999).
59. Lee, J. et al. Molar-scale formate production via enzymatic hydration of industrial off-gases. *figshare* https://doi.org/10.6084/m9.figshare.25433956.v2 (2024).

Acknowledgements

This research was supported by the C1 Gas Refinery Program and the Engineering Research Center Program through the National Research Foundation of Korea (NRF), funded by the Ministry of Science, ICT and Future Planning (2015M3D3A1A01064919 and 2020R1A5A1019631, respectively), and KEIT (1415184376).

Author contributions

Y.H.K. and S.M.K. conceived and planned all the experiments. S.M.K. performed the bioinformatic analysis and gene cloning. S.M.K., Jinhee Lee, B.W.J., H.W.H., E.G.P. and J.K. performed the biochemical characterization, kinetic analysis and feasibility evaluation, all under the supervision of Y.H.K., S.L., H.W.R., J.N., J.-G.N. and Jinwon Lee. S.M.K. performed the structural analyses. Y.H.K. and S.M.K. wrote and reviewed the paper.

Competing interests

The authors declare no competing interests.

Additional information

Extended data is available for this paper at https://doi.org/10.1038/s44286-024-00063-z.

Supplementary information The online version contains supplementary material available at https://doi.org/10.1038/s44286-024-00063-z.

Correspondence and requests for materials should be addressed to Suk Min Kim or Yong Hwan Kim.

Peer review information *Nature Chemical Engineering* thanks Michael Köpke and the other, anonymous, reviewer(s) for their contribution to the peer review of this work.

https://doi.org/10.1038/s44286-024-00063-z

Extended Data Table 1 | Catalytic properties of CODHs and FDHs

	Name	Mediator	Specific activity[a]	K_M for mediators	k_{cat}	k_{cat}/K_M
			(U·mg^{-1})	(mM)	(sec^{-1})	(mM^{-1}·sec^{-1})
CO oxidation	*Ch*CODH2	BV_{ox}	510 ± 23	1.4 ± 0.1	620 ± 7.3	430 ± 15
		EV_{ox}	290 ± 4.6	3.0 ± 0.02	300 ± 6.4	98 ± 2.1
		NAD^+	ND	ND	ND	ND
	*Ch*CODH2 A559W	BV_{ox}	1,400 ± 29	1.6 ± 0.05	1,500 ± 27	910 ± 14
		EV_{ox}	560 ± 8.5	2.6 ± 0.1	550 ± 5.1	210 ± 8.0
		NAD^+	ND	ND	ND	ND
	*Ch*CODH4	BV_{ox}	42 ± 0.36	1.3 ± 0.2	41 ± 1.9	32 ± 2.1
		EV_{ox}	17 ± 0.32	1.6 ± 0.1	19 ± 0.7	12 ± 0.52
		NAD^+	ND	ND	ND	ND
	*To*CODH	BV_{ox}	170 ± 1.9	2.2 ± 0.1	190 ± 1.6	84 ± 1.4
		EV_{ox}	61 ± 0.73	3.5 ± 0.2	63 ± 1.3	18 ± 0.62
		NAD^+	ND	ND	ND	ND
CO_2 reduction	*Me*FDH1	BV_{red}	1.3 ± 0.2	0.015 ± 0.003	2.0 ± 0.2	130 ± 3.5
		EV_{red}	66 ± 1.2	0.053 ± 0.004	120 ± 4.8	2,200 ± 79
		NADH	1.2 ± 0.1	0.028 ± 0.003	1.8 ± 0.1	65 ± 3.2
	*Rc*FDH	BV_{red}	ND	ND	ND	ND
		EV_{red}	4.2 ± 0.1	0.027 ± 0.002	6.2 ± 0.2	230 ± 11
		NADH	ND	ND	ND	ND
	*Ts*FDH	BV_{red}	ND	ND	ND	ND
		EV_{red}	ND	ND	ND	ND
		NADH	ND	ND	ND	ND

Kinetic properties of the associated enzymes were quantified under the given enzymatic reaction conditions. [a]Specific activities were determined at 20 mM mediator in sodium phosphate buffer saturated with CO (30 °C, pH 6.5). Values are the means ± standard variation, n = 3. * Kinetic data were assayed at 30 °C, pH 6.5. The kinetic parameters were calculated by fitting the initial rates obtained at six different BV/EV concentrations (0.0625–32 mM) to the Hanes–Woolf equation using SigmaPlot 10.0. All enzymatic activities were determined in triplicate (see details in the Methods section). † The values of k_{cat} were calculated from V_{max} for BV and EV. ND was noted when the specific activity was under 1 U·mg^{-1}.

nature portfolio

Corresponding author(s): Yong Hwan Kim

Last updated by author(s): Mar 20, 2024

Reporting Summary

Nature Portfolio wishes to improve the reproducibility of the work that we publish. This form provides structure for consistency and transparency in reporting. For further information on Nature Portfolio policies, see our Editorial Policies and the Editorial Policy Checklist.

Statistics

For all statistical analyses, confirm that the following items are present in the figure legend, table legend, main text, or Methods section.

n/a	Confirmed	
☐	☒	The exact sample size (*n*) for each experimental group/condition, given as a discrete number and unit of measurement
☐	☒	A statement on whether measurements were taken from distinct samples or whether the same sample was measured repeatedly
☒	☐	The statistical test(s) used AND whether they are one- or two-sided *Only common tests should be described solely by name; describe more complex techniques in the Methods section.*
☐	☒	A description of all covariates tested
☐	☒	A description of any assumptions or corrections, such as tests of normality and adjustment for multiple comparisons
☐	☒	A full description of the statistical parameters including central tendency (e.g. means) or other basic estimates (e.g. regression coefficient) AND variation (e.g. standard deviation) or associated estimates of uncertainty (e.g. confidence intervals)
☒	☐	For null hypothesis testing, the test statistic (e.g. *F*, *t*, *r*) with confidence intervals, effect sizes, degrees of freedom and *P* value noted *Give P values as exact values whenever suitable.*
☒	☐	For Bayesian analysis, information on the choice of priors and Markov chain Monte Carlo settings
☒	☐	For hierarchical and complex designs, identification of the appropriate level for tests and full reporting of outcomes
☒	☐	Estimates of effect sizes (e.g. Cohen's *d*, Pearson's *r*), indicating how they were calculated

Our web collection on statistics for biologists contains articles on many of the points above.

Software and code

Policy information about availability of computer code

Data collection	We have provided a full code availability statement in the manuscript.
Data analysis	We have provided a full code availability statement in the manuscript.

For manuscripts utilizing custom algorithms or software that are central to the research but not yet described in published literature, software must be made available to editors and reviewers. We strongly encourage code deposition in a community repository (e.g. GitHub). See the Nature Portfolio guidelines for submitting code & software for further information.

Data

Policy information about availability of data

All manuscripts must include a data availability statement. This statement should provide the following information, where applicable:

- Accession codes, unique identifiers, or web links for publicly available datasets
- A description of any restrictions on data availability
- For clinical datasets or third party data, please ensure that the statement adheres to our policy

We have provided a full data availability statement in the manuscript.

Research involving human participants, their data, or biological material

Policy information about studies with human participants or human data. See also policy information about sex, gender (identity/presentation), and sexual orientation and race, ethnicity and racism.

Reporting on sex and gender	N/A
Reporting on race, ethnicity, or other socially relevant groupings	N/A
Population characteristics	N/A
Recruitment	N/A
Ethics oversight	N/A

Note that full information on the approval of the study protocol must also be provided in the manuscript.

Field-specific reporting

Please select the one below that is the best fit for your research. If you are not sure, read the appropriate sections before making your selection.

☒ Life sciences ☐ Behavioural & social sciences ☐ Ecological, evolutionary & environmental sciences

For a reference copy of the document with all sections, see nature.com/documents/nr-reporting-summary-flat.pdf

Life sciences study design

All studies must disclose on these points even when the disclosure is negative.

Sample size	No statistical methods were used to predetermine the sample size. At least three independent experiments were performed in this work. Sample sizes were determined on the basis of previous experiments by considering biological and technical variabilities.
Data exclusions	No data were excluded in this work.
Replication	At least three independent experiments were performed to verify our results. All of the attempts were successful.
Randomization	Randomization was not applicable for the experiments performed, since no statistical comparisons were performed.
Blinding	Blinding was not relevant to our study, since no statistical comparisons were performed.

Reporting for specific materials, systems and methods

We require information from authors about some types of materials, experimental systems and methods used in many studies. Here, indicate whether each material, system or method listed is relevant to your study. If you are not sure if a list item applies to your research, read the appropriate section before selecting a response.

Materials & experimental systems

n/a	Involved in the study
☒	☐ Antibodies
☒	☐ Eukaryotic cell lines
☒	☐ Palaeontology and archaeology
☒	☐ Animals and other organisms
☒	☐ Clinical data
☒	☐ Dual use research of concern
☒	☐ Plants

Methods

n/a	Involved in the study
☒	☐ ChIP-seq
☒	☐ Flow cytometry
☒	☐ MRI-based neuroimaging

Plants

Seed stocks	N/A
Novel plant genotypes	N/A
Authentication	N/A